Setup for the calibration of current measuring systems under DC signals affected by ripple

Domenico Giordano,
Davide Signorino,
Istituo Nazionale di ricerca metrologica
INRIM
Torino, Italy
d.giordano@inrim.it
d.signorino@inrim.it

Antonio Delle Femine
Daniele Gallo
dept.of engeneering
University of Campania "Luigi Vanvitelli"
Aversa, Italy
antonio.dellefemine@unicampania.it
daniele.gallo@unicampania.it

***Abstract*—In recent years, the adoption of DC technology in power systems is attracting renewed interest from the technical-scientific side not only in traditional high voltage applications (HVDC) which allow more efficient transmission of large quantities of energy over large distances but also in low voltage DC networks (LVDC), which allow for more efficient and sustainable integration of renewable energy sources and battery storage systems. An obstacle to its widespread diffusion is the lack of traceable reference systems able to evaluate the performance of energy meters for billing purposes in operating conditions characterized by DC with AC components (up to hundreds of kHz). The present work proposes a methodology to calibrate current measuring systems experiencing DC with AC ripple providing the metrological traceability for this combined signal. The developed and tested archetype, here presented, proves the feasibility of the methodology.**

Keywords— DC Grid, DC Measurement, Calibration, Traceability, LVDC, HVDC, Power Quality, Ripple Measurement.

I. INTRODUCTION

DC technology has always been used in the history of electrical distribution. The first electrical distribution networks (back in 1882 by Edison) were based on DC voltage and current. Successively with the invention of transformers, AC systems took over thanks to their competitive advantage for their better performances in terms of energy efficiency. Excluding specific high-voltage applications like submarine power transmission [1] or rail transport electrification [2], typically implemented in DC; electrical power has been almost exclusively generated, transmitted and distributed in AC form for years. Nowadays, new technology for energy conversion re-enables DC distribution as a more energy-efficient solution. Most of the loads in modern houses (but even factories) are in DC (e.g. computers, monitors, home appliances, LED lights, e vehicles, etc...) [3], [4]. and also many RES (Renewable Energy Sources) are in DC (such as photovoltaics, fuel cells, batteries, and other energy storage elements) [5]. The conversion from DC source to AC distribution and again from AC to DC load entails losses that obviously negatively impact overall efficiency [6]. This situation has further worsened, considering that the ongoing diffusion of new technologies related to the electrification of mobility implies high DC loads distributed on the electrical grid. In fact, BEVs (Battery Electric Vehicles) can be charged directly in DC, especially the fastest charge technologies that require a DC connection. Moreover, the energy flux became bidirectional considering the new V2G (vehicle to grid) enabled systems, especially the Off-board V2G, which works purposely in DC to avoid the double conversion AC/DC and DC/AC.

Better integration of distributed RES can be achieved by adopting DC grids at medium and high voltage without any DC–AC conversion, with an improvement of the total system energy efficiency [5]. Moreover, with modern HVDC (High Voltage Direct Current) technology it is possible to provide more energy per square meter over greater distances with lower losses and less space requirements than High Voltage AC. Moreover, variable speed (wind) generators and large motor drives would benefit from connecting to DC feeders since only half of the power electronics are needed, compared to AC feeders [5]. Finally, there are numerous studies on converting existing AC lines into DC in order to enhance power transfer and provide greater power control, significantly improving power trading [7], [8].

However, the proliferation of DC technologies in the near future is not a straightforward task. Low-voltage direct current (LVDC) systems and grids should at least provide the same level of operational reliability, and safety as their counterpart AC systems to support consumer and market confidence.

In such a context, issues related to DC system operation, control, protection, and measurements need to be understood and resolved. Measurements are crucial to quantify energy and evaluate efficiency, helping designers and final customers make the best choices [9], and it is also essential to monitor the DC Power Quality (PQ) [10]. From a technical point of view, measuring electrical quantities in direct current can be more complex than expected. Some problems, like offset, are totally absent in AC, and other aspects like instrument bandwidth are not trivial. In fact, voltage and current in a DC power system are not perfectly constant, but they are both time-varying signals and deciding the needed bandwidth is not trivial. The presence of additional components with respect to the simple constant value is primarily due to the generation mechanisms of the DC power supply which typically involve the AC/DC conversion. Traditional passive converters normally produce low frequency fluctuation (ripple). But modern switching DC/DC, AC/DC, and DC/AC converters produce ripple at increasingly higher frequencies up to hundreds of kHz or more. Additional fluctuations and deviations in voltage and currents around the average DC value apply as a result of the occurrence of PQ phenomena. These phenomena include only transitory events related to failure such as short circuits or strikes but also common events that apply during normal operation such as sudden load insertion, time-varying or not linear absorption of power loads, intermittent generation by RESs, power unbalance among sources and loads, etc. The frequency range related to these phenomena can be very wide.

So, measuring a DC signal means measuring a signal that has main spectral components at a low frequency from DC to

a few Hz, spectral components at AC network frequency and its multiples (depending on the technology of rectifiers, or another kind of energy converters eventually present), but also spectral components up to hundreds of kHz, due to connected switching systems [11], [12].

Focusing on traceability, there is a considerable lack of metrological references for this kind of measurement. Considering current measurements, reference transducers are always calibrated for DC or AC, never for both [13]. To the best authors' knowledge, the CMC (Calibration and Measurement Capability) of the NMIs (National Metrology Institutes) are related to DC-only or AC-only quantities. Nevertheless, it is not possible to use the calibration certificate obtained with the DC standards for measurements of ripple at a frequency of some kHz. A calibration procedure, able to guarantee metrological traceability for actual DC signals, combining NMI available standards for DC and for AC, in order to build up a metrological infrastructure suitable for actual DC measurements is needed.

In the following, to go beyond the state-of-the-art before described, a methodology for the reference generation of DC current with superimposed AC ripple will be proposed. Section II describes the basic idea of the proposed approach, Section III focuses on a primary analysis of the systematic errors introduced by the setup. Then, section IV describes the electromagnetic simulation tool for the design of the current transformer (CT) devoted to the injection of the AC ripple and the CT archetype that has been realized to arrange the experiment that proves the proposed methodology and to verify the reliability of the numerical tool. Finally, section V provides preliminary considerations on a future design of a more performing DC-with-ripple reference generation system.

II. Proposed Approach

The aim of the proposed setup is to solve the traceability issues affecting DC signals with ripple. This problem becomes relevant in the presence of a shunt as a current sensor. For measuring systems that involve inductive DC transducers (e.g. hall effect, fluxgate sensors) the traceability to DC and AC signals can be easily guaranteed thanks to the galvanic separation between the pure DC and the AC circuit [14]; this approach cannot be applied to resistive shunts.

The proposed approach involves two different reference generation systems, parallel connected, which supply the device under test. Similar issue was faced for voltage in [15]. Fig. 1 provides a sketch of the proposed setup (in the following named ALFO). A DC generation system implemented by a calibrator supplying a trans-conductance amplifier provides the reference DC generation system. A current generator a shunt and a current transformer provide the reference AC generation system. The current sensor under test experiences a DC with overlapped AC ripple. The DC certification of the calibrator plus trans-conductance amplifier guarantees the traceability for the DC current component, while the AC calibration of the AC shunt and the CT guarantee the traceability for the AC ripple. The high parallel impedance of the DC trans-conductance amplifier (see circuit model of Fig. 2) forces the AC current injected by the CT to flow almost exclusively in the sensor under test, that is, the targeted behaviour in the desired approach. On the contrary, since there is a current divider formed by the resistance of the DUT and the secondary winding of the CT, a portion potentially not small of the current, supplied by the trans-conductance

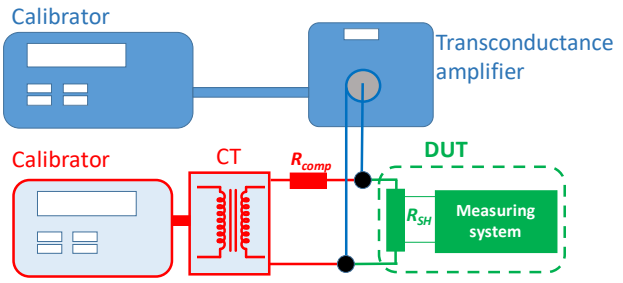

Figure 1. Scheme of the proposed approach

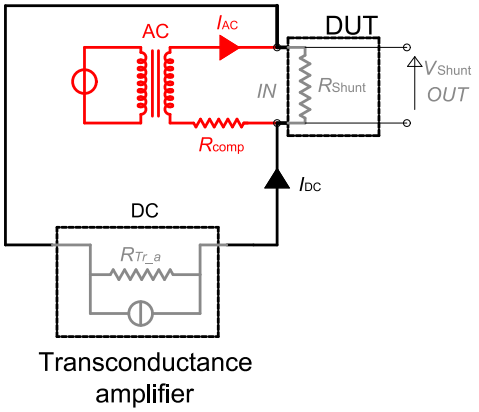

Figure 2 circuital scheme of the proposed method

amplifier, does not cross the DUT, entailing a remarkable systematic error. But this value can be limited by the presence of a compensation resistance R_{comp} series connected to the secondary circuit of the CT. Its value could be of hundreds of Ohm in order to make negligible the before mentioned systematic error. But, on the other side, a high value of such resistance implies a high ratio error of the CT. However, it is possible to find a compromise value which allows the application of the technique. To prove the feasibility of the proposed method, a CT archetype has been realized. The dynamics and frequency bandwidth of the calibration signals are limited for this first experiment to focus on feasibility. The maximum amplitude of the test signal is 50 A and 1.5 A for the DC and AC components respectively, the AC frequency range is limited to the 2 kHz – 6 kHz.

III. DC and AC Systematic Deviations Model

The current generated by the DC trans-conductance amplifier split in two parts due to the current divider constituted by the resistance of the shunt under test, R_{sh}, and the compensation resistance, R_{comp} (see Fig. 3). For this reason, the actual current injected in the DUT, $I_{R,DC}$, is lower than that provided by the DC reference chain (I_{DC}). Such considerations allow to quantify the systematic deviations as:

$$I_{R,DC} = I_{DC}\frac{R_{comp}}{R_{comp}+R_{sh}} = I_{DC}\cdot k_{DC} \qquad (1)$$

where I_{DC} is the current generated by the DC current generator and k_{DC} corrects the systematic error introduced by R_{comp}. k_{DC} is defined as:

$$k_{DC} = \frac{1}{1+{R_{sh}}/{R_{comp}}} \qquad (2)$$

To make negligible the systematic error due to the current divider, a high value of R_{comp} should be chosen.

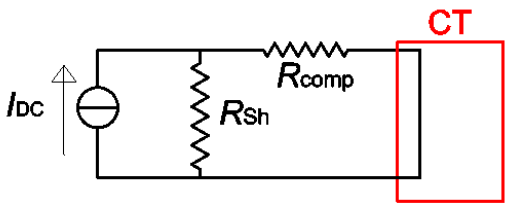

Figure 3. Current divider between the shunt undert test and the CT secondary circuit (secondary winding resistance is neglected) series connected with the compensation resistor R_{comp}

For instance, assuming a shunt under test with a rated current of 50 A, that provides a rated resistance of $R_{sh} = 16\ m\Omega$ and selecting R_{comp} of 1 Ω, the correction factor is $k_{DC} = 0.9843$ Ω/Ω. Such value rises to 0.9920 Ω/Ω with $R_{comp} = 2\ \Omega$.

The AC current component is provided to the DUT by an iron-core Current Transformer (CT). Considering turn ratio t, defined as the ratio between the number of primary (N_1) and secondary (N_2) turns, its scale factor is defined as:

$$\overline{k_{CT}} = \frac{\overline{I_{AC}}}{\overline{I_2}} = \frac{\overline{I_{AC}}}{\overline{I_2'} \cdot t} \tag{3}$$

where I_2 and I_2' are the current flowing in the secondary and the correspondent value at primary respectively. An approximated circuit model of the CT is provided in Fig. 4 (the winding stray inductance and resistance are neglected). The equivalent resistance at secondary (R_{load}) is the series of resistance R_{comp} and the resistance of the device under test, R_{sh}. The current I_2' is obtained by applying to I_{AC} the current divider rule between the magnetization impedance and the secondary impedance as seen at primary winding ($t^2 R_{load}$) and thus:

$$\frac{\overline{I_2'}}{\overline{I_{AC}}} = \frac{Z_p}{R_{load} \cdot t^2 + Z_p} \tag{4}$$

So, form (3), the complex scale factor can be calculated as:

$$\overline{k_{CT}} = \frac{1}{t} \cdot \frac{Z_p}{R_{load} \cdot t^2 + Z_p} \tag{5}$$

It is apparent that in this AC systematic deviation, a high value of R_{comp} worsens the AC ratio error, in contrast to what was found for the DC.

In addition, it is important to note that the DC current flowing in the secondary winding of the CT will introduce a magnetic bias in the iron-core with an increase of the magnetic field and the induction in turn. Consequently, the working point of the iron-core moves towards the saturation zone, activating the device's non-linearity, which becomes evident with a second harmonic distortion on the secondary current. Anyway, it is possible to compensate for this magnetic bias by injecting a DC current in the primary winding, such as to generate a magnetic flux opposite to the secondary one.

IV. CT Implementation and Analysis

To give a proof of feasibility of the proposed compensation technique, an archetype of a CT, suitable to be employed in the compensation scheme in fig. 1, was realized.

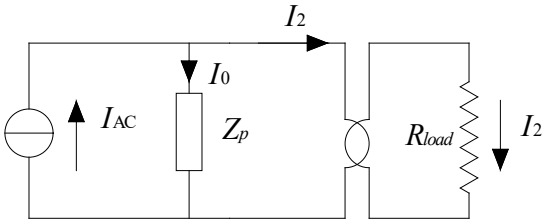

Figure 4. Simplified circuit model of the AC CT

The peculiarity of the proposed compensation technique makes it necessary to plan and carry out specific analyzes and characterization procedures of the CT. So, a model of the CT will be created and analyzed. Finally, a comparison between the model, tailored to the archetype, and the measurements from metrological characterization, will be provided.

The main construction features of the realized archetype of iron-core CT able to provide the AC current component to the DUT are summarized in TABLE I.

TABLE I. PARAMETER OF THE CT

N_2	30
N_1	20
t_{rated}	0.667
R_{load}	1.02 Ω
Iron-core	Mu-metal

The iron-core is a toroid 2 cm high; the external radius is 1.7 cm while the internal one is 1 cm. It has been selected mu-metal, an alloy of iron and nickel with high level magnetic characteristics; the relative permeability is of about $\mu_r = 50000$. The saturation induction is lower than the common silicon-iron; about 0.6 T. Fig. 5 provides a comparison between the B-H characteristic of the mu-metal (the blue curve) and the silicon-iron (the black curve). Considering the limited number of turns at primary ($N_1 = 20$) and the low magnetization current (guess values range from 8 mA to 30 mA), the magnetic field (H) is very low; it ranges from 1 A/m to 6 A/m, mu-metal provides, in this interval a higher permeability. This will guarantee a high value of Z_p and thus a low CT ratio error. To compute Z_p, a magnetic problem has been faced by following the finite element approach. The electromagnetic problem has been modelled using the FEMM 4.2 software. The 2D planar description of the geometry (see Fig. 6) has been considered suitable for this problem.

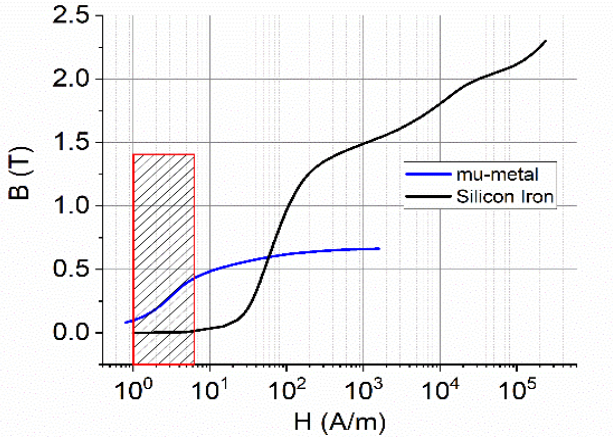

Figure 5. Comparison between magnetic characteristics of mu-metal and silicon-iron. The red box highlights the operating magnetic field range.

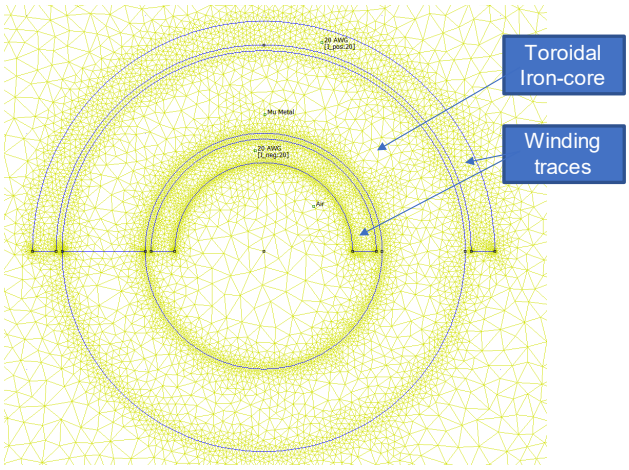

Figure 6. Geometry of the magnetic problem that involves a planar section of the toroidal iron-core and the projections of the primary winding.

A circular area filled with air wraps the magnetic choke. This reduces the boundary condition effects. Since the aim is the determination of the parallel impedance that simulates the magnetization inductance and the resistive element emulating the iron losses, only the primary winding is simulated. FEMM software provides the induced voltage which allows the determination of the impedance. Assuming that the longitudinal parameters (the winding stray inductance and resistance) are very lower compared with the parallel parameters of the transformer, the computed impedance is assumed equal to the parallel one. By a Python script that manages the FEMM software, the complex impedance Z_p, and the ratio error of the CT, defined as:

$$\varepsilon_{CT} = \left(\frac{k_{CT\_r}}{k_{CT}} - 1\right) \cdot 100 \qquad (6)$$

where k_{CT_r} is the scale factor measured by removing R_{comp} and supplying the primary current with 1 A at 6 kHz, which have been computed at different frequencies of the injected primary current. An average value of 0.015 A for the current injected in the primary circuit has been applied as input to the magnetic problem. The ratio error is defined as the deviation of the scale factor from the one at high frequency. At the increase of the frequency, the magnetization current tends to zero and thus the CT ratio tends towards the unit value.

A. CT characterization

The actual turns ratio t_a is obtained by removing R_{comp} applying only a sine waveform at 6 kHz to the primary CT, and measuring the primary and secondary current. An actual ratio of t_a = 0.6594 A/A has been found. Four tests have been performed in order to determine the CT archetype parameters (longitudinal and transversal parameters) and the associated ratio error. The measurement results have been compared with the model output in order to assess its reliability (see Fig.7).

- The stray parameters of the windings have been measured by performing a short-circuit test. An overall inductance of 22.2 µH and a resistance of 154 mΩ have been measured with the Philips PM 6303 RCL meter; 8.88 µH, 61.6 mΩ for the primary winding and 13.2 µH, 92.4 mΩ for the secondary one.
- To quantify the parallel impedance of the CT no-load tests at different frequencies and for different input currents have been performed. A block scheme of the measurement setup is shown in Fig. 8. The Fluke Calibrator 5730A provides the AC current at primary, the primary voltage

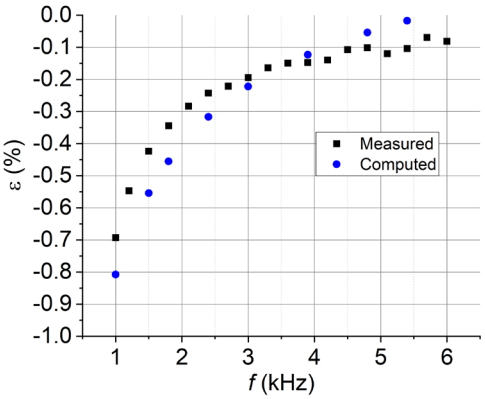

Figure 7. Comparison between measured and computed ratio error of the CT archetype.

and the secondary one is acquired by the National Instrument Data Acquisition (NI DAQ) module NI 9239 (±10 V, 50 kS/s/ch, 24-Bit, Simultaneous input). The impedance estimation has been computed by varying the frequency in the range 1 kHz – 6 kHz and the injected current amplitude from 5 mA to 70 mA. A chromatic map summarizing the parallel impedance variability is provided in Fig.11. Because of the resistive-inductive characteristics of the impedance, it increases with frequency. At the increase of the injected current, the magnetic field increases, the working point moves towards the linear H-B characteristics (see in Figure 5) with a consequent increase of the magnetic permeability (the slope of the H-B curve) thus of the self-inductance of the primary winding. Following the self-inductance behavior, the impedance increases up to 30 mA, for higher current, the iron-core moves towards the saturation region with a decrease of the permeability, thus a decrease of the inductance and consequently a decrease of the impedance. For current value higher than 40 mA the saturation effects become more evident in the impedance reduction. For the analyzed frequency and current ranges, the impedance ranges from about 9 Ω to 55 Ω.

- The third test is devoted to the determination of the CT ratio error. The adopted setup is shown in Fig. 9. The ratio error behaviour versus supply frequency, for a primary current of 1 A, 1.5 A and 2 A, is provided in Fig. 10. The ratio error behavior reflects the frequency behavior of the parallel impedance (); namely, at the increase of the parallel impedance, the ration error defined in (6) reduces. Moreover, the decrease of the ratio error at the increase of the primary current is due to the fact that for such primary current, the no-load one (that is the current flowing in the parallel impedance) is in the range 10 mA –

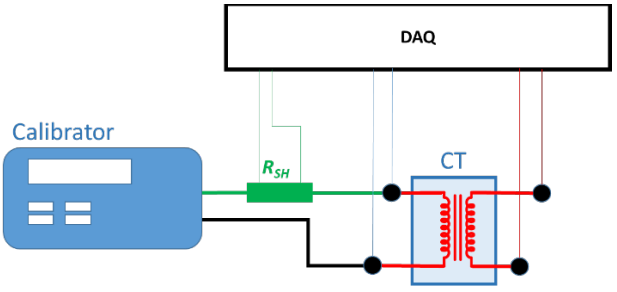

Figure 8. Setup for the open-circuit test

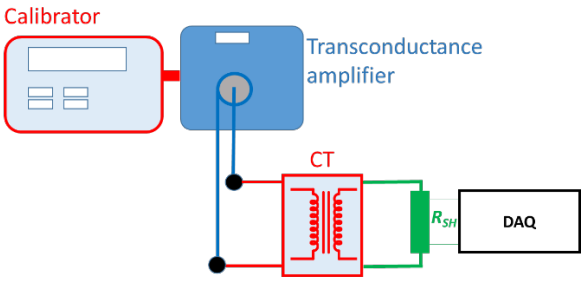

Figure 9. Setup for the CT ratio error evaluation

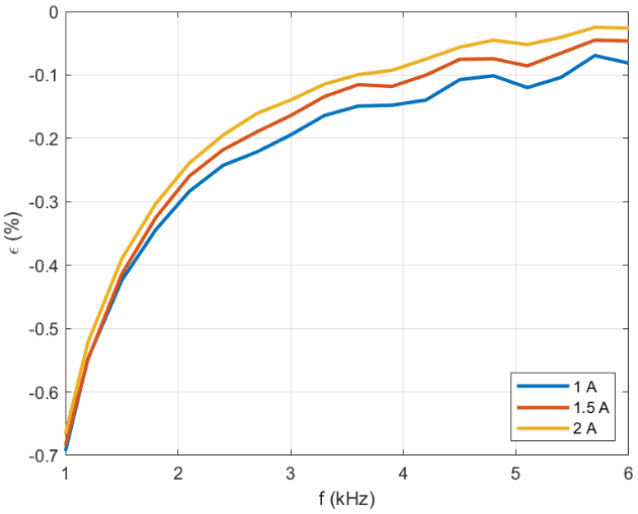

Figure 10. Measured frequency behavior of the CT ratio error for different primary current

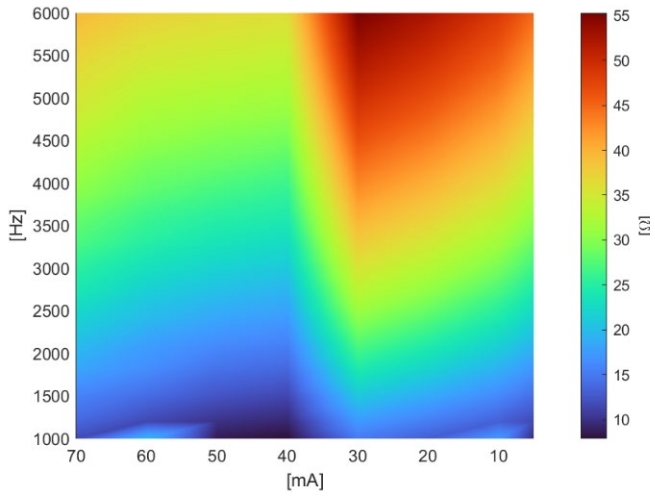

Figure 11. Z_p versus frequency and amplitude of I_0

30 mA in which (see Fig. 11) for a fixed frequency, the impedance increases at the increase of the no-load current and, consequently, in accordance with (6), the ratio error decreases.

- Finally, a test to verify the distortion effect caused by the presence of an undesired DC component injected in the secondary winding has been performed. As stated before, part of the DC current will flow in the secondary winding of the current transformer, despite the presence of R_{comp} (see the previous section and Figure 3). This will lead to a harmonic distortion; the amplitude of the second harmonic of the AC secondary current has been measured as an indicator of such distortion.

The measurement setup for this test is reported in Fig. 12. The archetype current transformer has been fed with a 1 kHz input signal on the primary winding. Simultaneously on the secondary side a DC has been injected to emulate the real operating conditions, and to evaluate the impact of this influence quantity. Finally, a DC current has been injected on the primary side too, in order to compensate for the magnetic bias. Measurement results are shown in TABLE II: on the first raw the amplitude of the second harmonic with no DC at secondary is reported. On the second raw, when 667 mA DC is injected in the secondary, the second harmonic rises to -27 dB. By applying a DC compensation current to the primary, it has been possible to reduce the 2 kHz component to -80 dB; thus, the THD of the AC signal drastically improves, becoming even better than the initial situation with no DC (-54 dB). Note that the 667 mA test value corresponds to the current divider on a total DC of 50 A generated by the amplifier in normal operating conditions. The value of DC current at the primary that minimizes the undesired second harmonic (2 kHz) at the secondary results in 800 mA.

TABLE II. EFFECT OF THE DC COMPONENT INJECTED ON THE SECONDARY WINDING

	Primary		*Secondary*	
	Ip_{fund} @1 kHz (mA)	*Ip @DC (mA)*	*Is @DC (mA)*	*Ip^{2h} @2kHz (dB)*
No DC	446	0	0	-54
DC at secondary	378	0	667	-27
Compensation at primary	454	800	667	-80

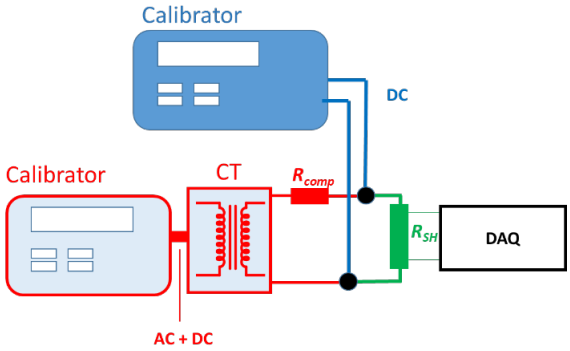

Figure 12. Setup for implementing the DC compensation at primary circuit

V. CONSIDERATIONS FOR THE FURTHER DESIGN

From the preliminary experimental results, it can be stated that the proposed model has proved to be a valuable tool for the design of the calibration setup. A first action to move toward the final project and to improve the CT archetype performances is the increase of the iron-core section. This will lead to an increase of the magnetization inductance thus of the parallel impedance Z_p. This produces, in turn, a reduction of the ratio error (6) as quantified and shown in Fig. 13.

The ratio error has been determined by taking the computed scale factor (provided by (5)) at 6 kHz as rated one.

The ratio error reduces from -0.24 % with an iron-core 2 cm high to 0.08 % by tripling the core height. By fixing the core high to 6 cm, in order to reduce the systematic error on the DC side due to the current divider between R_{comp} and R_{sh} (Fig. 3), R_{comp} is increased to 2 Ω. For this configuration, at 3 kHz, the ratio error moves to -0.23% while the correction coefficient to be applied to the output current of the transconductance amplifier, k_{DC}, increases to 0.992 A/A (with R_{comp} = 1 Ω was k_{DC} = 0.98 A/A). The improvement of the ratio error can be reached by increasing the turn number on the primary circuit avoiding the saturation condition; on the other side, the higher the number of turns the higher the stray capacitive coupling among turns [16] with a limitation on the CT bandwidth at high frequency.

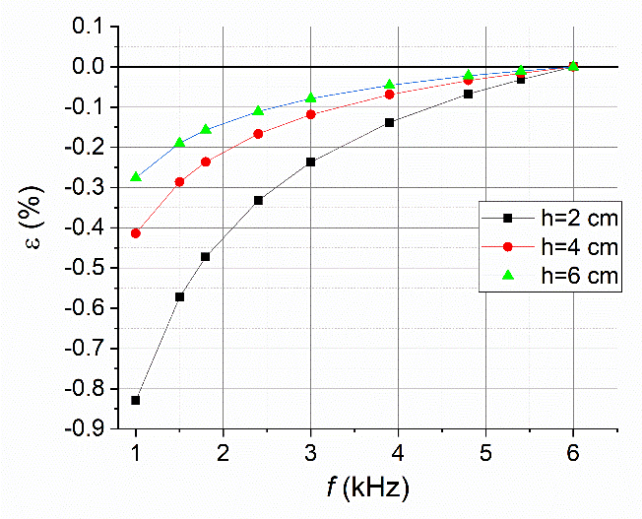

Figure 13. Frequency behavior of CT ratio error for different iron-core sections

VI. CONCLUSIONS

A methodology to generate a reference signal composed by a DC with superimposed ripple for the calibration of current measuring systems, named ALFO, has been described. This method, once fully implemented, will guarantee metrological traceability for signals composed of predominant DC and smaller AC components, typical of real-world applications. A preliminary analysis of the systematic errors and their corrections have been discussed. A model for the design of such setup has been developed and verified by the comparison with the measurements performed on an archetype of CT. The setup, which represents a proof of concept of the ALFO method, allows the generation of a DC current up to 50 A and a sinusoidal ripple in the frequency range 1 kHz – 6 kHz and an AC current dynamic of 1 A – 2 A. The CT archetype has a ratio error lower than 0.5 % in the range 2 kHz – 6 kHz. Finally, preliminary considerations have been provided for a further design of a more complete setup.

ACKNOWLEDGMENT

The work here presented has been supported in part by the European Metrology Programme for Innovation and Research (EMPIR), co-funded by the European Union's Horizon 2020 research and innovation programme and the EMPIR participating states, under Project 20NRM03 DC grids, and in part from the project 22NRM04 e-TRENY that has received funding from the European Partnership on Metrology, co-financed by the European Union's Horizon Europe Research and Innovation Programme and from by the Participating States.

REFERENCES

[1] H. N. Le and E. Tedeschi, "Comparative Evaluation of AC and DC Power Distribution Systems for Underwater Vehicles Based on Multiobjective Optimization Techniques," in IEEE Transactions on Power Delivery, vol. 36, no. 6, pp. 3456-3465, Dec. 2021, doi: 10.1109/TPWRD.2020.3043054.

[2] D. Giordano, D. Signorino, A. D. Femine, D. Gallo and G. Cipolletta, "Power Quality in DC railway systems," 2021 IEEE 11th International Workshop on Applied Measurements for Power Systems (AMPS), Cagliari, Italy, 2021, pp. 1-6, doi: 10.1109/AMPS50177.2021.9586027.

[3] K.-T. Mok, M.-H. Wang, S.-C. Tan, and S.Y. Ron Hui, "DC electric springs – A technology for stabilizing DC power distribution systems," *IEEE Trans. Power Electron.*, vol. 32, no. 2, pp. 1088-1105, Feb. 2017.

[4] A. Q. Huang, M. L. Crow, G. T. Heydt, J. P. Zheng, and S. J. Dale, "The future renewable electric energy delivery and management (freedm) system: The energy internet," Proceedings of the IEEE, vol. 99, no. 1, pp. 133–148, 2011.

[5] J.J. Justo, F. Mwasilu, J. Lee, and J.-W. Jung, "AC-microgrids versus DC-microgrids with distributed energy resources: A review", *Renewable and Sustainable Energy Reviews*, vol. 24, pp. 387-405, Aug. 2013.

[6] G. W. Arnold, "Challenges and opportunities in smart grid: A position article," Proceedings of the IEEE, vol. 99, no. 6, pp. 922–927, 2011.

[7] A. Elahidoost and E. Tedeschi, "Expansion of offshore HVDC grids: An overview of contributions, status, challenges and perspectives," in *Proc. 2017 IEEE 58th Int. Scientific Conf. Power Electr. Eng. of Riga Technical University*, Riga, Latvia, Oct. 2017, pp. 1-7.

[8] G. Arcia-Garibaldi, et al., "Supergrids in Europe: Past studies and AC/DC transmission new approach," in *Proc. 2017 IEEE Manchester PowerTech*, Manchester, UK, Jun. 2017, pp. 1-6.

[9] C. Wang, M. Song, W. Fei, T. Zhao, X. Liu and Y. Xu, "Design of Current Ripple Measurement System for Highly Stabilized Magnet Power Supply," 2022 International Conference on Machine Learning, Control, and Robotics (MLCR), Suzhou, China, 2022, pp. 183-187, doi: 10.1109/MLCR57210.2022.00041.

[10] G. Van den Broeck, J. Stuyts, and J. Driesen, "A critical review of power quality standards and definitions applied to DC microgrids," *Appl. Energy*, vol. 229, pp. 281–288, Nov. 2018.

[11] B. Djokić and H. Parks, "Measurement of Voltage, Current and Power at Distorted Waveforms," in IEEE Instrumentation & Measurement Magazine, vol. 24, no. 3, pp. 11-17, May 2021, doi: 10.1109/MIM.2021.9436100.

[12] X. Yue, L. Mengyu, C. Weimin, Y. Li, Z. Jiangming and N. Linna, "Research on the Effect of Ramp Waveform with Ripple on Electric Energy Measurement in Subway DC Power Supply," 2020 IEEE 3rd International Conference on Automation, Electronics and Electrical Engineering (AUTEEE), Shenyang, China, 2020, pp. 1-5, doi: 10.1109/AUTEEE50969.2020.9315675.

[13] G. Frigo and J. Braun, "Measurement Setup for a DC Power Reference for Electricity Meter Calibration," 2022 20th International Conference on Harmonics & Quality of Power (ICHQP), Naples, Italy, 2022, pp. 1-5.

[14] G. Frigo and M. Agustoni, "Development of a Transfer Standard for DC Power Quality Reference Systems," 2022 IEEE 12th International Workshop on Applied Measurements for Power Systems (AMPS), Cagliari, Italy, 2022, pp. 1-6.

[15] M. Zucca, M. Modarres, U. Pogliano and D. Serazio, "1-kV Wideband Voltage Transducer, a Novel Method for Calibration, and a Voltage Measurement Chain," in IEEE Transactions on Instrumentation and Measurement, vol. 69, no. 4, pp. 1753-1764, April 2020, doi: 10.1109/TIM.2019.2912589.

[16] D. Giordano, G. Crotti, P. S. Letizia and D. Palladini, "Stray Parameter Evaluation of Voltage Transformers for PQ Measurement in MV Applications," 2022 20th International Conference on Harmonics & Quality of Power (ICHQP), Naples, Italy, 2022, pp. 1-6.